Journal of Materials Chemistry C

ROYAL SOCIETY OF CHEMISTRY

PAPER

Cite this: J. Mater. Chem. C, 2020, 8, 8804

Tuning the edge-on oriented ordering of solution-aged poly(3-hexylthiophene) thin films†

Md Saifuddin,[a] Mala Mukhopadhyay,[b] Arindam Biswas,[a] Lara Gigli,[c] Jasper R. Plaisier[c] and Satyajit Hazra*[a]

Received 25th April 2020,
Accepted 18th May 2020

DOI: 10.1039/d0tc02031a

rsc.li/materials-c

Structural evolution of solution-aged poly(3-hexylthiophene) [P3HT] thin films during thermal annealing (TA) was studied using complementary *in situ* X-ray reflectivity (XR) and *ex situ* atomic force microscopy (AFM) and optical absorption (UV-Vis) techniques to understand the possibility of obtaining enhanced edge-on oriented (EO) ordering for better device properties. The presence of P3HT nanofibers (NFs), which were formed through π–π stacking within solution during aging, is evident in the films. Such NFs are well-organized near the film–substrate interface and less organized near the film–air interface due to the respective slow and fast evaporation rates of the solvent during spin-coating. Accordingly, prominent EO ordering (*i.e.* the electron density contrast between the polymer backbone and side chains is maximum, $\Delta\rho \approx \Delta\rho_m$) near the substrate and negligible ordering (*i.e.* $\Delta\rho \rightarrow 0$) near the top surface took place following the standard decay function: $\Delta\rho(z) = \Delta\rho_m \exp(-z/\zeta)$, where the critical decay length, ζ, is the measure of the out-of-plane ordering. TA fails to improve the $\Delta\rho_m$-value, *i.e.* the EO ordering near the substrate and also the total crystalline aggregates or NFs, rather deteriorates both, when annealed near the melting temperature of P3HT. TA improves the ζ-value, *i.e.* the EO ordering of the more out-of-plane region due to thermal energy induced alignment of the NFs; however, lack of improvement of the EO ordering near the substrate is of concern. A relatively low viscous polymer solution and low spin-coating speed play important roles in the formation of a smooth film–substrate interface and better EO ordering near that interface. Though solvent vapor annealing (SVA) fails to improve the structure, the combination of SVA and TA, *i.e.* SVTA, improves the in-plane EO ordering near the substrate (*i.e.* the $\Delta\rho_m$-value) along with the out-of-plane ordering (*i.e.* the ζ-value) of the film. Such improvements, which are probably through the alignment and growth of NFs, promoted by SVTA induced proper diffusion, are of immense importance for obtaining better device properties.

1 Introduction

Conjugated polymer films have attracted massive attention as active layers in opto-electronic devices, such as light-emitting diodes (LEDs), photovoltaics (PVs), and thin-film transistors (TFTs) due to their elusive structural and morphological properties, which give rise to intriguing charge transport characteristics.[1–5] Among the large family of π-conjugated polymers, poly(3-alkylthiophenes) [P3ATs] are particularly effective in TFT applications due to their lower cost, easier fabrication and substantial mobilities.[6–9] The charge carrier mobilities of P3AT devices strongly depend on the polymer crystallinity, crystal orientation and interfacial morphology.[7,10] P3AT thin films are semicrystalline in nature, where the crystalline domains, separated by amorphous portions, are organized into two main orientations: edge-on, in which π–π stackings are parallel to the substrate, and face-on, in which π–π stackings are perpendicular to the substrate.[7,11] Many groups have pointed out that increasing the edge-on oriented (EO) crystals with extended inter-molecular π–π stacking and long intra-molecular conjugation length is likely to improve the field effect mobility.[12–14]

Poly(3-hexylthiophene) [P3HT] is one such P3AT, which has been studied extensively due to its promising field effect mobility. Several methods have been employed to enhance the charge carrier mobilities of P3HT thin films, such as tuning the molecular weight,[15] casting the film using high boiling point solvents,[12] treating the dielectric layer with self-assembled monolayers,[16] changing the deposition techniques,[9,17] and post-deposition treatments (namely thermal annealing and solvent vapor annealing).[18,19] Recently, solution aging (*i.e.* combined effect of sonication and aging) has been used as a new method

[a] Saha Institute of Nuclear Physics, HBNI, 1/AF Bidhannagar, Kolkata 700064, India. E-mail: satyajit.hazra@saha.ac.in
[b] B R A Bihar University, Muzaffarpur, 842001, India
[c] Elettra – Sincrotrone Trieste S. C. p. A., 34149 Basovizza, Trieste, Italy

† Electronic supplementary information (ESI) available. See DOI: 10.1039/d0tc02031a

to enhance the charge carrier mobility of a film.[20,21] The appreciably higher mobilities (~10-fold improvement) observed in the solution-aged P3HT films compared to the pristine films[21] have been correlated with the crystallinity, fiber length, grain boundaries and conjugation length of polymer chains, as studied by the atomic force microscopy (AFM) and optical absorption techniques. However, it can be noted that the film-morphology, as obtained from AFM (which essentially provides the film-topography, *i.e.* surface morphology), can differ considerably from the actual morphology, especially near the film–substrate interface *i.e.* the buried interface. The structure and morphology of this buried interface are known to play very crucial roles in the charge transport of a TFT and its device performances.[22,23] Unfortunately, no attempt has been made, so far, to understand the structure and morphology of the buried interface in the solution-aged films. Moreover, the effect of post-deposition treatments on the solution-aged films is unknown. It is thus necessary to understand the structure of the buried interface and also to check the possibility of obtaining further enhanced EO ordering, if any, combining solution aging and post-deposition treatments, which can be well performed using the X-ray reflectivity (XR) technique.[24–27] The XR technique essentially provides an electron density profile (EDP), *i.e.* in-plane $(x - y)$ average electron density (ρ) as a function of depth (z) in high resolution.[28–30] From the EDP it is possible to estimate the film thickness, the electron density, the surface and interfacial roughness, the presence of layering in the film, the structural arrangement near the film–substrate interface and their evolution.[31–34]

In this article, the synchrotron XR technique has been utilized to understand the out-of-plane structures and EO ordering of solution-aged spin-coated P3HT thin films and their evolution due to thermal annealing (TA), solvent vapor annealing (SVA) and solvent vapor thermal annealing (SVTA). A high brilliance synchrotron source has been utilized to obtain relatively wide dynamic range XR data with better resolution, which helps to remove uncertainties in the data analysis. Further, complementary AFM and optical absorption techniques have been used to obtain the information about the topography, the conjugation length and the overall crystallinity of the films. Indeed, better EO ordering near the film–substrate interface is observed in the as-grown films, prominent structural modification along the out-of-plane direction compared to the in-plane direction is found during TA and SVA treatments, and quite significant enhancement of ordering along both the in-plane and out-of-plane directions is found during SVTA. An attempt has been made to understand the observed structural ordering and its evolution in terms of growth parameters. Also, possible implications of such interesting structures on the charge carrier mobility are discussed.

2 Experimental

P3HT (average M_W 54 000–75 000 and regioregularity >98%) was purchased from Sigma-Aldrich and used as received. P3HT solutions were prepared by dissolving the polymer in toluene (obtained from Merck). Two concentrations (c = 4 and 8 mg ml^{-1}) of P3HT in toluene solutions were prepared. The solutions were sonicated for 10 min and annealed at 50 °C for 5 min, and then aged for 72 h. Prior to the film deposition, Si and quartz glass wafers (size about 12 × 12 mm^2) were sonicated in acetone and ethanol solvents to remove organic contaminants. Films were then formed using a spin-coater (SCS 6800 Spin Coater)[30] at a fixed spinning time (60 s) but for different spinning speeds (ω) after placing the solution onto the substrate and waiting for a min. The films prepared with c = 4 mg ml^{-1} and ω = 2500 rpm, c = 4 mg ml^{-1} and ω = 2000 rpm, and c = 8 mg ml^{-1} and ω = 5000 rpm on Si substrates are labeled S1, S2 and S3, respectively. Similarly, the films prepared with c = 4 mg ml^{-1} and ω = 2500 rpm on quartz glass substrates are labeled G1. Separate S1 films, used for XR and AFM studies, are renamed $S1_X$ and $S1_A$, respectively. All films were subsequently annealed at 70 °C for 15 min under vacuum conditions, which will be referred to as as-cast films.

XR measurements of the films were carried out using a synchrotron source (MCX beamline, Elettra)[35,36] at an energy of 10 keV (*i.e.* wavelength, λ_X = 1.24 Å). The beamline was equipped with a diffractometer, which has a four-circle goniometer and a flat sample stage. The latter has two circular and three translational (X, Y, and Z) motions. A Kapton window-based cell was placed on the flat sample stage. Scattered intensities were recorded using a scintillator detector behind a set of receiving slits. In the XR technique, data were taken under specular conditions; that is, the exit angle is equal to the incident angle θ. Under such conditions there exists a nonvanishing wave vector component, q_z, which is given by $(4\pi/\lambda_X)\sin\theta$ with a resolution of 0.001 Å^{-1}. The XR measurements of all the films were carried out in a vacuum, after placing them inside the cell. For the *in situ* TA measurements the temperature of the cell was further controlled (from room temperature to 220 °C) using a temperature controller. For the *in situ* SVA measurements limited toluene vapor was introduced inside the pre-vacuum cell from a small conical flask containing toluene solvent using an attached stop cock. Similarly, for the *in situ* SVTA measurements limited toluene vapor was introduced once inside the pre-vacuum cell and heating was carried out simultaneously only at relatively low temperatures (at 130 °C) to avoid any possible combustion.

The detailed topographic images of the as-cast solution-aged P3HT thin film and after TA at different temperatures were collected using an atomic force microscope (CSI Nano-Observer). Such AFM images were collected in tapping mode for different scan sizes and in different portions of the sample to get statistically meaningful information about the topography. Processing and analysis of AFM images were carried out using Gwyddion software. Optical absorption spectra of the as-cast solution-aged P3HT thin film and after TA at different temperatures were collected using a UV-Vis spectrophotometer (JASCO, V-630).

3 Results and discussion

3.1 Topography of the solution-aged P3HT thin film

AFM images of a solution-aged P3HT thin film ($S1_A$) in the as-cast condition and after TA at different temperatures are shown in Fig. 1. The fibrous nature of the film is clearly evident

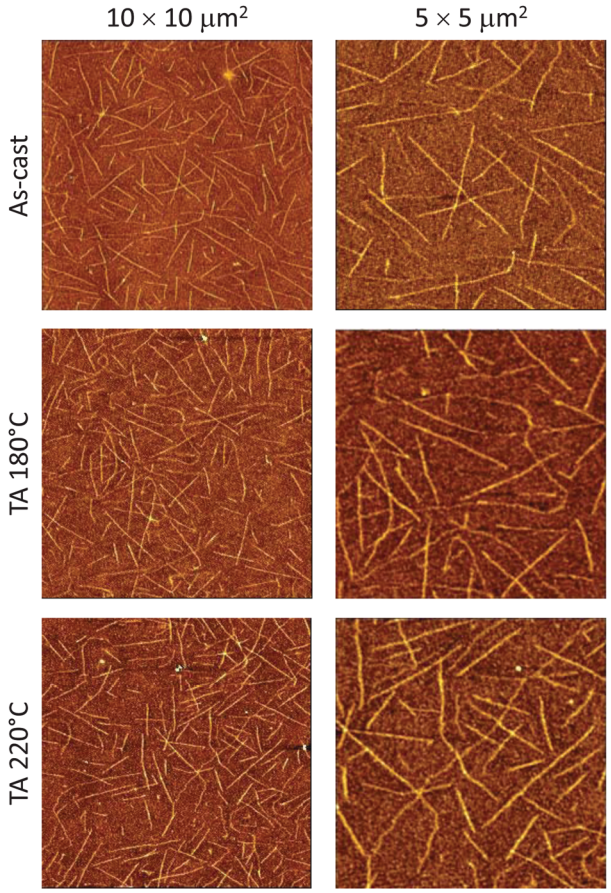

Fig. 1 AFM images in two different scan sizes of a solution-aged P3HT thin film ($S1_A$) in the as-cast condition and after thermal-annealing (TA) at different temperatures.

from the topographical images. Also, it is evident that such fibers having a typical length and width are randomly distributed in-plane. The observation of such fibers in the topography of the as-cast film can be related to the growth of nanofibers (NFs) due to π–π stacking of the polymer chains during solution-aging. The length of the NF is related to the extension of such stacking, while the width is related to the polymerization length.[37] To obtain detailed information about the NFs, the topographical images have been analyzed quantitatively (as shown in Fig. S1 of ESI†). The average length (L_{NF}), width (W_{NF}), height (H_{NF}) and coverage (C_{NF}) of the P3HT NFs obtained from the analysis are listed in Table 1. The length of the NFs is found in the order of microns, which is quite large compared to that observed before.[21] This improvement in the length of P3HT NFs is quite interesting and may be related to the solvent used (namely toluene in place of chloroform), which however needs further verification. Negligible changes in the size of the NFs after TA can be correlated with their stability, while a very small increase in the values of W_{NF} and C_{NF} after TA can be correlated with the thermal energy induced reorganization of the NFs, as discussed later.

Table 1 Average length (L_{NF}), width (W_{NF}), height (H_{NF}) and coverage (C_{NF}) of NFs on the solution-aged P3HT thin film ($S1_A$) surface in the as-cast condition and after TA at different temperatures, as obtained from the analysis of the AFM images

Treatment	L_{NF} [μm]	W_{NF} [nm]	H_{NF} [nm]	C_{NF} [%]
As-cast	2.1	56	2.0	10
TA-180 °C	2.0	58	2.0	14
TA-220 °C	2.0	59	2.0	16

3.2 Optical absorption of the solution-aged P3HT thin film

The UV-Vis absorption spectra of a solution-aged P3HT thin film (G1) in the as-cast condition and after TA at different temperatures are presented in Fig. 2. The photophysics of the P3HT thin film can be well described using a weakly interacting H-aggregate model,[14,38] which deals with the interchain excitonic delocalization along π–π stacking, neglecting the excitonic motion along each polymer chain.[39] Accordingly, each absorption spectrum can be categorized into two parts – lower wavelength part, which consists of intrachain (π–π* transition) states (around $\lambda \approx 470$ nm) arising from disordered polymer chains, and prominent higher wavelength part, which consists of weakly interacting H-aggregated states arising from the crystalline domains (here NFs) of the film.[14] Further, the peak at $\lambda \approx 520$ nm can be assigned to intrachain π–π* transition of P3HT and the peaks at $\lambda \approx 560$ nm and 603 nm can be assigned to interchain π–π stacking interactions.[40,41]

The weakly interacting H-aggregate model, which provides peaks at $\lambda \approx 603$ nm, 560 nm and 520 nm due to 0–0, 0–1 and 0–2 transitions,[14,42–44] can be used to obtain quantitative information about the average conjugation length and the crystalline quality of the film. The intensity of the 0–0 transition in the absorption spectra is known to reduce by the increased exciton coupling. The coupling strength (J_0) or the free exciton bandwidth ($W = 4J_0$), which is the measure of the conjugation length along the polymer backbone and intrachain order, can

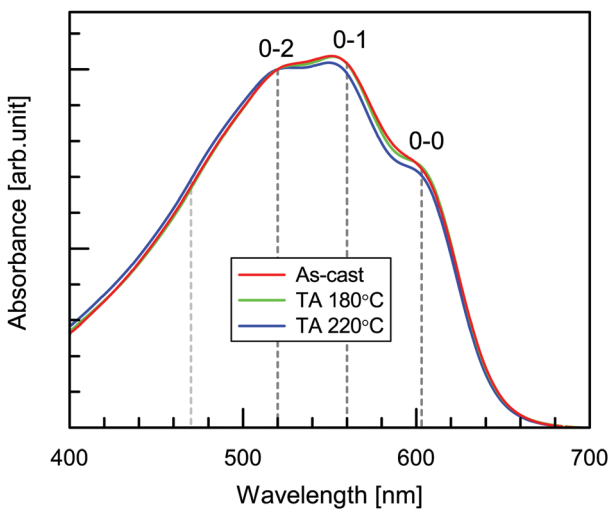

Fig. 2 UV-Vis spectra (normalized at the 0–2 transition) of a solution-aged P3HT thin film (G1) in the as-grown condition and after thermal-annealing (TA) at different temperatures. Positions of the transition peaks, corresponding to the weakly interacting H-aggregate model, are indicated.

be expressed in terms of the intensity ratio of the 0–0 and 0–1 transitional peaks as[14,38]

$$\frac{I_{0-0}}{I_{0-1}} \approx \frac{\left(1-0.24W/E_p\right)^2}{\left(1+0.073W/E_p\right)^2} \quad (1)$$

where E_p is the vibrational energy of the C=C symmetric stretch (assumed to be 0.18 eV).[42] An increase in the I_{0-0}/I_{0-1} ratio corresponds to a decrease in the excitonic coupling, therefore an increase in the conjugation length (or planarity) and the degree of intrachain order.[45,46] Here, the value of $I_{0-0}/I_{0-1} \approx 0.75$, which corresponds to a value of $W \approx 80$ meV, is found to remain almost unchanged for different spectra, suggesting no appreciable change in the conjugation length in the film with TA. On the other hand, no significant change in the absorption spectrum of the film TA at 180 °C is observed compared to that of the as-cast film, while the intensities of the 0–0 and 0–1 peaks for the film TA at 220 °C are found to decrease slightly compared to those of the as-cast film. Franck–Condon fit is generally used to obtain the percentage of aggregates in the solution or film.[14,39] Here, a slightly modified expression is used to fit the spectra (as shown in Fig. S2 of ESI†), which indicates that the amount of aggregates or NFs (~68%) in the solution-aged P3HT thin film decreases (~3%) or the polymer chain disorder increases after TA at high temperature.[41]

3.3 EDP of the solution-aged P3HT thin film

3.3.1 Effect of TA. XR profiles of a solution-aged P3HT thin film ($S1_X$), predominantly during TA, *i.e.* during heating, cooling and SVA followed by heating and cooling at different temperatures are shown in Fig. 3, 4 and 5, respectively. Oscillations or Kiessig fringes,[47] which are the measure of the total film thickness ($D_K = 2\pi/\Delta q_K$, where Δq_K is the difference between two consecutive Kiessig fringes), are evident in all the XR profiles.[30] The sharp peaks around $q_z \approx 0.38$ and 0.76 Å^{-1}, which correspond to the 1st and 2nd order pseudo Bragg peaks of the EO ordering, are also evident in all the XR profiles. The positions of such peaks (q_B and $2q_B$) provide the layer thickness ($d_B = 2\pi/q_B$), while the width of the peak (Δq_B) provides the crystallite size or the critical ordering length (ξ) of the EO ordered structures along the *z*-direction. The latter can be estimated using the standard Scherrer's formula, $\xi \approx 4\pi C/(\Delta q_B \cos\theta_B)$, where $C \approx 0.9$ is a dimensionless Scherrer constant and θ_B is the Bragg angle.[11] The evolution of the Kiessig fringes, pseudo Bragg peak and its width with TA is very apparent from the XR profiles (in Fig. 3, 4 and 5).

In order to understand the evolution properly, the parameters such as D_K, ξ and d_B, estimated from the XR profiles, are plotted as a function of temperature (T) in Fig. 6 for heating, cooling and subsequent SVA, heating and cooling cycles. The value of d_B is found to increase with heating, which can be related to the relaxation and thermal expansion of the polymer side chains. This also leads to an increase in the value of D_K. The increase in the value of ξ with heating suggests the improvement in the size of the EO crystallites along the *z*-direction due to reorganization. The values of D_K and d_B are found to decrease with subsequent cooling, which can be correlated with the contraction (*i.e.* reversible thermal expansion). The value of ξ

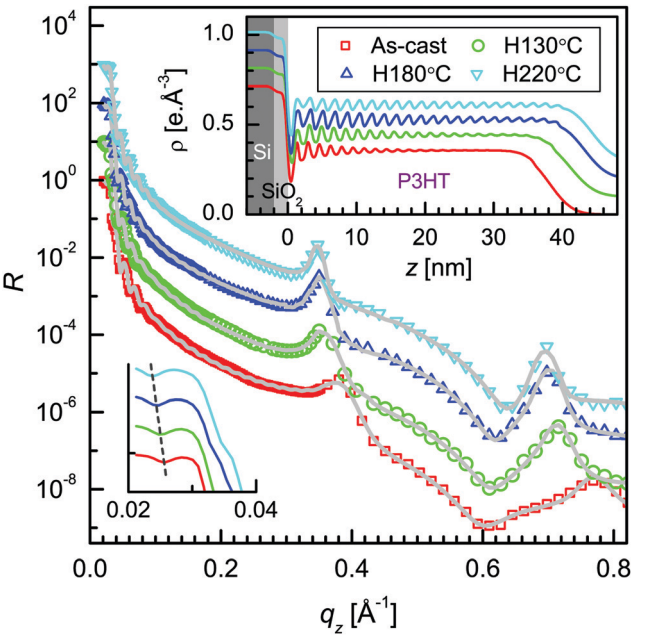

Fig. 3 Evolution of XR profiles (different symbols) and analyzed curves (solid lines) of a solution-aged P3HT thin film ($S1_X$) during heating (H) at different temperatures. The positions of the critical wave-vector of the film ($q_{c,film}$) are indicated by a dashed line in the zoomed view of the selected portion. Inset: Corresponding analyzed EDPs. Curves and profiles are shifted vertically for clarity.

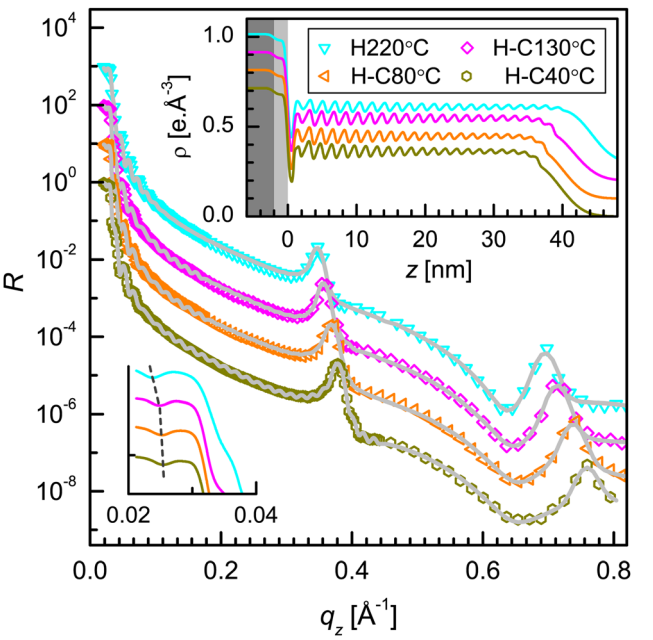

Fig. 4 Evolution of XR profiles (different symbols) and analyzed curves (solid lines) of the solution-aged P3HT thin film ($S1_X$) during cooling (C) at different temperatures after heating. The positions of the critical wave-vector of the film ($q_{c,film}$) are indicated by a dashed line in the zoomed view of the selected portion. Inset: Corresponding analyzed EDPs. Curves and profiles are shifted vertically for clarity.

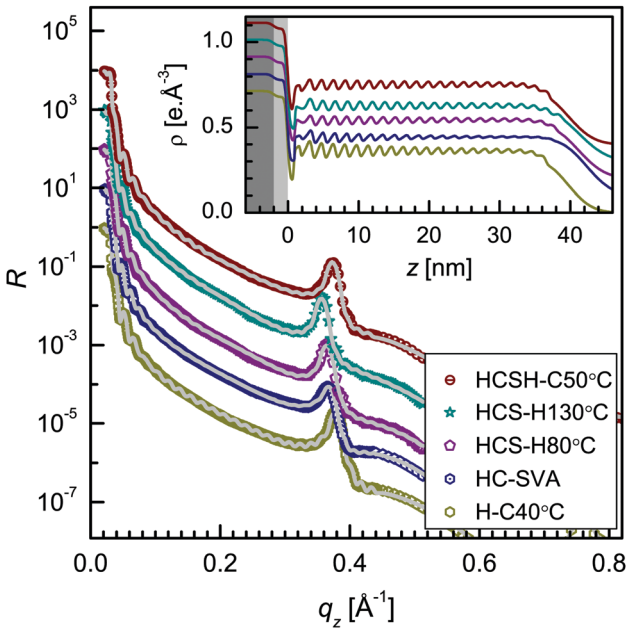

Fig. 5 Evolution of XR profiles (different symbols) and analyzed curves (solid lines) of the solution-aged P3HT thin film ($S1_X$) due to SVA after heating and cooling, and subsequent heating and cooling at different temperatures. Inset: Corresponding analyzed EDPs. Curves and profiles are shifted vertically for clarity.

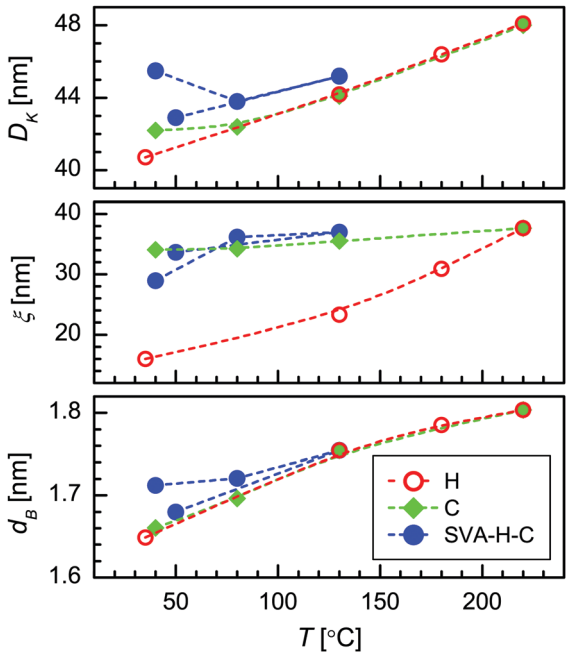

Fig. 6 Evolution of the film-thickness (D_K), the layer-thickness (d_B) and the critical ordering length (ξ) of the solution-aged P3HT thin film ($S1_X$) with temperature (T) during heating (H), cooling (C) and subsequent SVA, heating and cooling (SVA–H–C).

is found to remain almost the same on cooling, which can be correlated with the irreversible ordering. This observation is important as it can help in obtaining improved ordering in the film at room temperature. On the other hand, the observed increase in the values of D_K and d with subsequent SVA can be correlated with the polymer expansion due to the solvent diffusion inside the thin film, while the decrease in the value of ξ with SVA can be correlated with the deterioration in the ordering due to the solvent induced polymer dissolution. The values of D_K, ξ and d_B are found to decrease, increase and remain unchanged, respectively with subsequent heating at low temperatures, which can be correlated with the competitive effect between solvent evaporation and polymer expansion. Upon further heating at high temperatures and subsequent cooling, the parameters (d_B, D_K, and ξ) are found to behave similar to that of the first heating and cooling cycle, suggesting not much change or improvement in the structure or ordering of the film due to the additional SVA followed by heating and cooling cycle.

To get further information about the structure of the film, especially about the EO ordering, the XR data were analyzed quantitatively using the matrix method after incorporating roughness at each interface.[26,27] For the analysis, each film of thickness D was divided into a number of bilayers after incorporating an interfacial layer above the substrate,[30,48] where each bilayer of thickness d consists of a polythiophene backbone containing a high electron density (ρ_b) layer of thickness d_b and alkyl side chains containing a low electron density (ρ_c) layer of thickness d_c. The interfacial layer was considered to take care of the effect of the substrate surface energy on the growth of the film. Even then it was not possible to fit the XR data properly. To overcome this problem, further variation of the electron density contrast ($\Delta\rho = \rho_b - \rho_c$) along the z-direction was considered. Owing to the fact that the slow evaporation of the solvent near the film–substrate interface (*i.e.* larger time) is likely to help the organization of the polymers and their ordering there, while the fast evaporation of the solvent near the film–air interface (*i.e.* lesser time) is likely to restrict the organization of the polymers and their ordering at top, the variation of ρ_b and ρ_c as a function of depth (z) can be expressed as

$$\rho_b(z) = \rho_a + (d_c/d_b)\Delta\rho_a \exp(-z/\zeta) \quad (2)$$

$$\rho_c(z) = \rho_a - \Delta\rho_a \exp(-z/\zeta) \quad (3)$$

where ρ_a is the average electron density, $(1 + d_c/d_b)\Delta\rho_a = \Delta\rho_m$ is the maximum electron density contrast and ζ is the critical decay length. Here, d_c/d_b (>1) is used because the variation of ρ_b is greater than the variation of ρ_c w.r.t. the average value ρ_a. A large value of $\Delta\rho_m$ is related to better in-plane ordering towards the film–substrate interface and a large ζ-value suggests better out-of-plane ordering, which is related to the improvement of the in-plane ordering more towards the film–air interface. The information of the critical wave vector of the film, $q_{c,film}$ (as shown in the zoomed view of the selected portion of the XR profiles in Fig. 3 and 4), was used to obtain the starting value of ρ_a for the analysis of the respective XR data. It can be noted that although the analysis of the XR profiles of P3HT thin films was carried out before, none has collected and/or used the 2nd order Bragg peak data for the fitting.[22,49] However, the consideration of the 2nd order Bragg peak, in particular, and the higher q_z-range

XR data, in general, is quite important for removing the uncertainties in the data analysis and obtaining the near unique EDP, which were considered here. Instrumental resolution in the form of a Gaussian function and a constant background were also included at the time of data analysis.[33] The best fit XR profiles along with the corresponding EDPs thus obtained are presented in Fig. 3–5. The relevant parameters such as ρ_a, $\Delta\rho_m$, ζ, d, D, the interfacial roughness (σ_{in}) and the top surface roughness (σ_{ts}) for the solution-aged P3HT thin film ($S1_X$) during different treatments, as obtained from the analyzed EDPs, are listed in Table 2. The corresponding values of ξ (as presented in Fig. 6) are also included in Table 2 for comparison.

A dip near the film–substrate interface, observed in the EDP, suggests that the attachment of the film (*i.e.* predominantly EO NFs) with the substrate is through alkyl side chains. A small value of σ_{in} indicates smooth attachment of those alkyl side chains, while a high value of σ_{ts} confirms the presence of random NFs on the surface with in-plane variations in their effective heights. The values of both the parameters, and hence the respective natures of the film, remain almost unchanged during TA. The values of d obtained from EDPs (Table 2) follow well the values of d_B obtained directly from the pseudo Bragg peaks (Fig. 6), while the values of D obtained from EDPs (Table 2) correct the slightly overestimated values of D_K obtained directly from the Kiessig fringes (Fig. 6). Nonetheless, the variation of D with T follows the same pattern as that of D_K. The variation of ρ_a with T follows the opposite nature to that of D, as expected, to maintain the materials conserved.

Let us now discuss the parameters $\Delta\rho_m$ and ζ, which are of real importance in understanding the ordering of the system. The value of $\Delta\rho_m$ remains unchanged on heating up to 180 °C but decreases on further heating at 220 °C. This indicates that the in-plane ordering towards the film–substrate interface remains unchanged with TA except at high temperatures, where it decreases. This means that TA does not promote either the lateral growth or the number of EO NFs near the film–substrate interface; rather, it deteriorates the ordering at high temperatures probably due to the melting of P3HT polymer. The ζ-value, on the other hand, was found to increase with the heating temperature. This suggests an increase in the edge-on orientation along the z-direction due to the thermal energy induced reorientation and/or translation of NFs. The thermal energy induced growth of NFs can be ruled out as no appreciable increase in the aggregates was estimated from the optical absorption spectra. During cooling, the value of $\Delta\rho_m$ increases to recover some of the deteriorated ordering but not up to the mark, while the value of ζ decreases little bit but improves appreciably compared to the as-cast film. Thus through a cycle of TA, an appreciable increase in the EO ordering takes place due to the reorganization of the NFs. Such an improvement does not take place near the film–substrate interface, rather deteriorates, if annealed at high T (consistent with the UV-Vis results). The overall increase is mainly due to the improvement in the subsequent EO ordering along the z-direction (the effect of which on the top is consistent with the AFM results). Further SVA reduces the values of $\Delta\rho_m$ and ζ significantly, which means that SVA deteriorates the ordering both along the in-plane and out-of-plane directions. Though subsequent TA improves the EO ordering, it could not recover the ordering entirely.

3.3.2 Effect of SVA. XR profiles of the S3 thin film, predominantly during SVA, that is during swelling with time, deswelling and subsequent heating and cooling at different temperatures are shown in Fig. 7 and 8. The evolution of D_K, d_B and ξ due to SVA is shown in Fig. 9. SVA is found to increase the values of d_B and D_K due to the diffusion of solvent molecules

Table 2 Parameters, such as the average electron density (ρ_a), the maximum electron density contrast ($\Delta\rho_m$), the interfacial roughness (σ_{in}), the top surface roughness (σ_{ts}), the bilayer thickness (d), the total film thickness (D), the critical decay length (ζ) and the critical ordering length (ξ), of the solution-aged P3HT thin films during different treatments, as obtained from the XR data analysis

Sample	Treatment	ρ_a [e Å^{-3}]	$\Delta\rho_m$ [e Å^{-3}]	σ_{in} [nm]	σ_{ts} [nm]	d [nm]	D [nm]	ζ [nm]	ξ [nm]
$S1_X$	As-cast	0.35	0.10	0.3	2.6	1.63	38.2	3.8	16.0
	H130 °C	0.33	0.10	0.3	2.9	1.75	41.1	6.2	23.3
	H180 °C	0.32	0.10	0.3	2.6	1.78	43.3	10.2	30.9
	H220 °C	0.31	0.05	0.3	2.6	1.80	44.4	14.6	37.6
	H-C130 °C	0.32	0.07	0.3	2.9	1.75	41.4	14.5	35.5
	H-C80 °C	0.33	0.08	0.3	2.7	1.70	39.3	11.5	34.2
	H-C40 °C	0.34	0.08	0.3	2.7	1.65	38.9	11.2	34.0
	HC-SVA	0.32	0.05	0.3	2.9	1.69	42.2	7.4	29.0
	HCS-H80 °C	0.33	0.04	0.3	3.0	1.71	41.2	13.3	36.1
	HCS-H130 °C	0.33	0.06	0.3	3.3	1.75	41.4	17.0	37.0
	HCSH-C50 °C	0.34	0.06	0.3	2.9	1.67	39.3	11.5	33.7
S3	As-cast	0.33	0.04	0.7	3.4	1.61	60.7	4.0	16.1
	S10min	0.32	0.03	0.8	3.4	1.66	88.3	1.4	12.5
	S20min	0.32	0.03	0.8	3.4	1.68	91.2	1.5	11.6
	S30min	0.32	0.03	0.8	3.4	1.70	91.2	1.5	11.6
	DS5min	0.33	0.04	0.9	3.3	1.60	75.0	1.6	14.5
	DS-H80 °C	0.34	0.04	0.5	3.4	1.68	64.3	1.9	16.0
	DS-H130 °C	0.33	0.04	0.5	3.5	1.76	66.0	3.6	18.5
	DSH-C80 °C	0.33	0.04	0.5	3.4	1.71	65.2	4.8	18.0
S2	As-cast	0.34	0.14	0.3	2.5	1.63	42.7	3.0	16.0
	During SVTA	0.32	0.15	0.3	2.9	1.75	45.4	4.6	25.0
	After SVTA	0.34	0.19	0.3	2.7	1.66	43.8	4.5	24.0

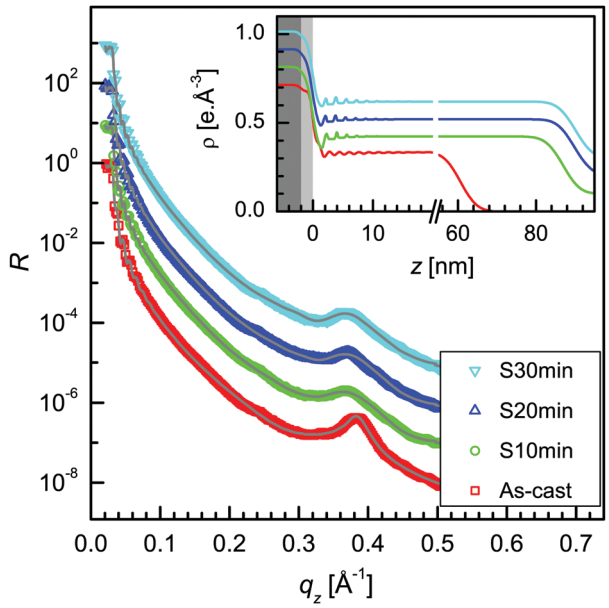

Fig. 7 Evolution of XR profiles (different symbols) and analyzed curves (solid lines) of a solution-aged P3HT thin film (S3) during SVA (or swelling) for different durations. Inset: Corresponding analyzed EDPs. Curves and profiles are shifted vertically for clarity.

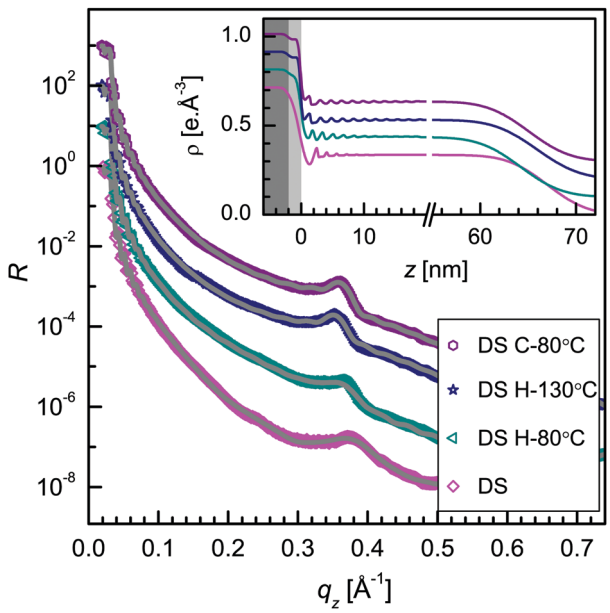

Fig. 8 Evolution of XR profiles (different symbols) and analyzed curves (solid lines) of the solution-aged P3HT thin film (S3) after deswelling and consequent heating and cooling. Inset: Corresponding analyzed EDPs. Curves and profiles are shifted vertically for clarity.

inside the polymer in the thin film. However, the increase of D_K is found to be more compared to that of d_B, suggesting that the diffusion of the solvent inside the disordered polymer is more compared to the NFs. This can be correlated with the relatively better stability of P3HT NFs even in the presence of a good solvent, which is likely as NFs are formed within a good solvent with time. The D_K is found to increase very fast initially

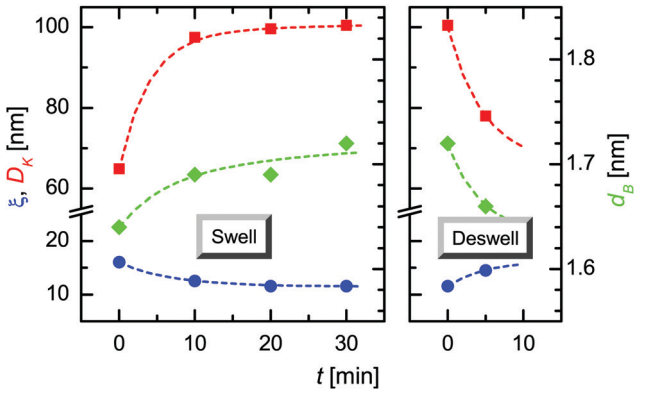

Fig. 9 Evolution of D_K, ξ and d_B for the solution-aged P3HT thin film (S3) due to SVA (or swelling) and deswelling.

(within 10 min) and then saturates gradually. The fast increase is related to the dissolution of the disordered polymer and saturation at a relatively lower value is related to the restricted dissolution of NFs and/or diffusion of limited solvent vapor. SVA of the thin film swells the polymers, which deteriorates the ordering of the film, as evident from the decrease of the ξ-value with time. Deswelling leads to a decrease of d_B and D_K values due to the evaporation of solvent molecules, whereas it recovers the ξ-value slightly.

The analyzed XR data (using eqn (2) and (3)) and the corresponding EDPs of the solution-aged P3HT thin film (S3) are shown in Fig. 7 and 8. The analyzed parameters are listed in Table 2. The values of σ_{in} and $\Delta\rho_m$ are found to be quite high and low, respectively, compared to those of sample $S1_X$. It can be noted that the sample S3 is made of a high concentration polymer solution and at high spinning speed. The high concentration makes the solution more viscus, while the high speed only allows less time to organize the P3HT NFs. The combination of these two is likely to make the attachment of the film with the substrate less smooth (thus more rough) and the subsequent arrangement of the NFs, less organized (*i.e.* less ordered). With SVA, the values of $\Delta\rho_m$ and ζ decrease, while that of σ_{in} increases, which indicates further deterioration in the ordering and the attachment of the film. The subsequent deswelling revives the structural ordering but not up to the mark. Further TA cycle actually revives the ordering of the film. In fact, it improves the ordering of the film little bit and film–substrate interface remarkably compared to the as-cast film.

3.3.3 Effect of SVTA. XR profiles and analyzed curves of the S2 thin film and corresponding EDPs during SVTA are shown in Fig. 10. The parameters obtained from the XR data analysis are listed in Table 2. It can be noted that most of the parameters behave similar to those of the $S1_X$ film, except that the value of $\Delta\rho_m$ is found to be more compared to that of the $S1_X$ film, which suggests that even a small decrease in the spinning speed improves the organization of the NFs and hence the ordering towards the film–substrate interface. Such ordering is found to improve further during SVTA (*i.e.* combined swelling and heating) treatment and even further during subsequent deswelling and cooling. Comparatively, less improvement in

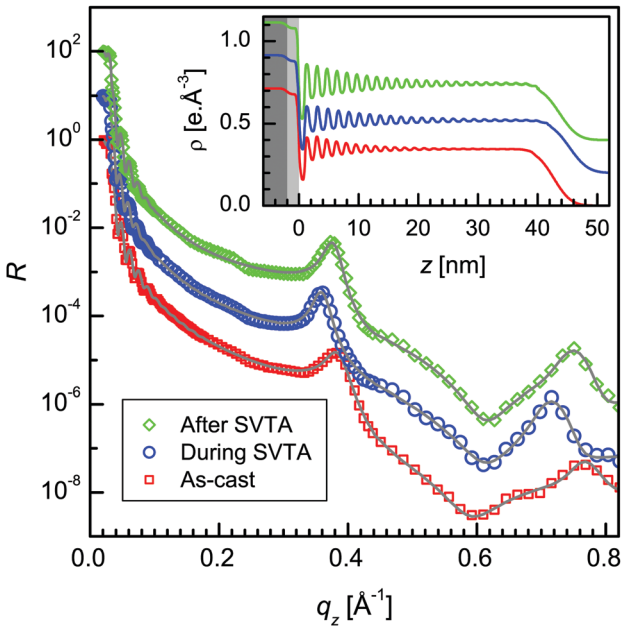

Fig. 10 Evolution of XR profiles (different symbols) and analyzed curves (solid lines) of the solution-aged P3HT thin film (S2) during SVTA (heating in the presence of solvent vapor) and after SVTA (due to cooling and deswelling). Inset: Corresponding analyzed EDPs. Curves and profiles are shifted vertically for clarity.

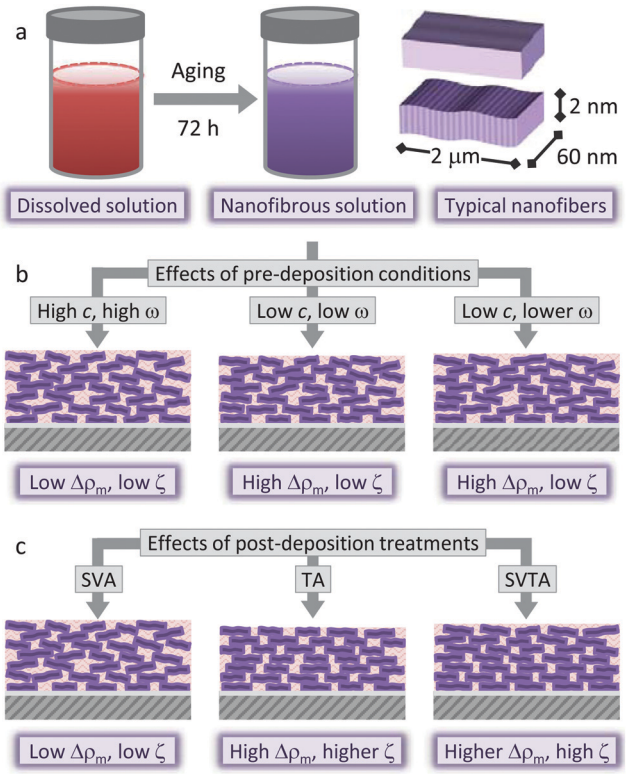

Fig. 11 Schematic illustration of the growth and organization of P3HT NFs. (a) Conversion of a well-dissolved (orange color) polymer solution to a nanofibrous (purple color) solution on aging, with typical size and shapes of the EO NFs. (b) Effects of pre- and during-deposition conditions, namely polymer concentration (c) and spin-coating speed (ω), on the film-structures, *i.e.* on the in-plane ($\Delta\rho_m$) and out-of-plane (ζ) EO ordering of the NFs, on solid substrates. (c) Effects of post-deposition treatments, namely SVA, TA and SVTA, on the same film-structural parameters.

the ordering of the film along the z-direction is observed (from the values of ζ and ξ) during the SVTA cycle.

3.4 Growth and organization of P3HT nanofibers

Let us now try to understand and model the growth and organization processes of P3HT NFs. Using the information obtained from the complementary techniques, the growth and organization of P3HT NFs can be modeled, as shown schematically in Fig. 11. The sonication and heating of the solution dissolve the polymer (Fig. 11a, orange color), while the subsequent cooling initiates the nucleation process, which on aging promotes the π–π stacking to form a nanofibrous solution (Fig. 11a, purple color) probably due to the increase in the supersaturation condition of the solution.[50] The sonication followed by heating seems to impose some restriction in the nucleation process, and hence in the number of nucleation sites, which in turn helps to form comparatively long NFs[21] on aging. Also, based on the Hansen solubility parameter ($\Delta\delta$), toluene is more likely to behave as a poor (or theta) solvent at room temperature, which can prefer the polymer–polymer interactions and the polymer coil contraction to initiate the nucleation and growth of NFs.[44]

The spin-coating deposits the NFs onto the solid substrate, which are predominantly EO with some preferred size and shapes (Fig. 11a). The initial organization of such NFs depends on the concentration (c) or the effective viscosity (η) of the solution and the spinning speed (ω) or the effective evaporation rate (E) of the solvent (shown in Fig. 11b). Also, it depends on the difference (ΔE) or gradient ($\Delta E/\Delta D$) in the evaporation rate of the solvent between the solution–substrate and the solution–air interfaces. The large η and E values restrict the diffusion, the organization and the ordering of the NFs, which then create a rough film–substrate interface, as evident in the S3 thin film of large c and ω values. On the other hand, the small η and/or E values enhance the organization time and/or the diffusion of the NFs to promote EO ordering (large $\Delta\rho$-value), which also creates a smooth film–substrate interface (small σ_{in}-value), as evident in the S1 and S2 thin films of small c and ω values. The smaller E value further enhances the diffusion and the organization of the NFs to create better EO ordering (larger $\Delta\rho$-value), as evident in the S2 thin film of smaller ω value. The slow evaporation near the film–substrate interface allows more time to organize the NFs and promotes better EO ordering (larger $\Delta\rho$-value), and the fast evaporation at the film–air interface provides little time to organize the NFs and creates negligible ordering ($\Delta\rho \rightarrow 0$) and very large roughness (σ_{ts}-value), while the varying (increasing) evaporation, in between, forms gradually changing (decaying) ordering (Fig. 11b) of the form $\Delta\rho(z) = \Delta\rho_m \exp(-z/\zeta)$, as observed in all the thin films.

The post-deposition treatment usually supplies energy to the film, which can impact on the NFs and the film-structure (shown in Fig. 11c). The SVA results in a rapid swelling of the thin film mainly through the dissolution of the disordered part

of the film, which then increases the film-thickness and deteriorates the EO ordering of the NFs, as evident for the S3 thin film. On the other hand, the TA, which supplies the thermal energy to the film, fails to improve the $\Delta\rho_m$-value, *i.e.* the EO ordering near the substrate and also the total crystalline aggregates or NFs, rather deteriorates both, when annealed near the melting temperature of P3HT, as evident for the $S1_X$, $S1_{AX}$ and G1 thin films. Such TA, however, improves the ζ-value, *i.e.* the EO ordering of the more out-of-plane region due to thermal energy induced alignment (through reorientation and/or vertical displacement) of the NFs. The lack of improvement of the maximum EO (*i.e.* in-plane) ordering at a particular height is of real concern towards its betterment in the device performances as observed before.[51] Finally, the combination of SVA and TA, *i.e.* the SVTA, improves the in-plane EO ordering near the substrate (*i.e.* the $\Delta\rho_m$-value) along with the out-of-plane ordering (*i.e.* the ζ-value) of the film. Similar improvements in the in-plane and out-of-plane ordering upon SVTA were also observed recently for the poly(3-dodecylthiophene) thin films.[48] Such improvements, in the present P3HT film, are probably through both reorientation and growth of NFs. In the case of SVTA, the thermal energy in the presence of limited solvent vapor not only promotes the reorganization and reorientation of the P3HT NFs but also promotes the unfavorable coil-to-rod conformational transformation of the P3HT polymer chains and their unfavorable π–π stacking (both of which require a negative entropy change)[11] around the existing NFs, similar to that observed in the solution, during aging.[52]

4 Conclusions

Complementary XR, AFM and UV-Vis spectroscopic techniques were utilized to observe the growth and evolution of the P3HT NFs within thin films upon TA, SVA and SVTA. Fibrous structures on the surface of the film were conveniently observed through AFM, whereas the overall crystallinity or the amount of NFs and their conjugation length were obtained through optical absorption study. Analysis of XR data or EDPs allows us to figure out the EO ordering of NFs both along the in-plane and out-of-plane directions and also the structures of the interfaces. Such information, which is quite unique to the XR technique and distinctive from other techniques, is important for understanding the device properties. It is quiet clear that the TA favors the alignment (through orientation and/or displacement) of the NFs but not their size (due to the poor diffusion of P3HT chains). Thus TA cannot improve the EO ordering near the film–substrate interface, where it was already better, rather towards the top parts, where the EO ordering was initially poor. The ordering becomes worse during SVA due to the swelling of the film and further deswelling cannot recover the ordering. The EO ordering of P3HT NFs is found to improve during SVTA (*i.e.* combined swelling and heating) treatment and even further during subsequent deswelling and cooling through alignment (reorientation and/or displacement) and growth (*i.e.* π–π stacking), which are of utmost importance for achieving better device performances.

Conflicts of interest

There are no conflicts to declare.

Acknowledgements

The authors thank Mr G. Sarkar for his help in AFM and XR measurements, Ms Soma Roy for her help in UV-Vis measurements and Prof. M. Mukherjee for extending the AFM facility. The financial support received from DST and Elettra under the Indo-Italian PoC to carry out XR experiments at the MCX beamline of Elettra is thankfully acknowledged. M. S. acknowledges the University Grant Commission (UGC), India, and A. B. acknowledges the Council of Scientific & Industrial Research (CSIR), India, for providing research fellowships.

References

1 J. H. Burroughes, D. D. Bradley, A. R. Brown, R. N. Marks, K. Mackay, R. H. Friend, P. L. Burns and A. B. Holmes, *Nature*, 1990, **347**, 539–541.
2 K. M. Coakley and M. D. McGehee, *Chem. Mater.*, 2004, **16**, 4533–4542.
3 R. J. Kline and M. D. McGehee, *J. Macromol. Sci., Part C: Polym. Rev.*, 2006, **46**, 27–45.
4 A. Facchetti, *Chem. Mater.*, 2010, **23**, 733–758.
5 J. R. Reynolds, B. C. Thompson and T. A. Skotheim, *Conjugated Polymers: Properties, Processing, and Applications*, CRC Press, 2019.
6 H. Sirringhaus, N. Tessler and R. H. Friend, *Science*, 1998, **280**, 1741–1744.
7 H. Sirringhaus, P. Brown, R. Friend, M. M. Nielsen, K. Bechgaard, B. Langeveld-Voss, A. Spiering, R. A. Janssen, E. Meijer and P. Herwig, *et al.*, *Nature*, 1999, **401**, 685–688.
8 H. Yan, Z. Chen, Y. Zheng, C. Newman, J. R. Quinn, F. Dötz, M. Kastler and A. Facchetti, *Nature*, 2009, **457**, 679–686.
9 S. Agbolaghi and S. Zenoozi, *Org. Electron.*, 2017, **51**, 362–403.
10 R. J. Kline, M. D. McGehee and M. F. Toney, *Nat. Mater.*, 2006, **5**, 222–228.
11 I. Roy and S. Hazra, *RSC Adv.*, 2015, **5**, 665–675.
12 J.-F. Chang, B. Sun, D. W. Breiby, M. M. Nielsen, T. I. Sölling, M. Giles, I. McCulloch and H. Sirringhaus, *Chem. Mater.*, 2004, **16**, 4772–4776.
13 R. J. Kline, M. D. McGehee, E. N. Kadnikova, J. Liu, J. M. Fréchet and M. F. Toney, *Macromolecules*, 2005, **38**, 3312–3319.
14 J. Clark, C. Silva, R. H. Friend and F. C. Spano, *Phys. Rev. Lett.*, 2007, **98**, 206406.
15 R. J. Kline, M. D. McGehee, E. N. Kadnikova, J. Liu and J. M. Frechet, *Adv. Mater.*, 2003, **15**, 1519–1522.
16 D. H. Kim, Y. D. Park, Y. Jang, H. Yang, Y. H. Kim, J. I. Han, D. G. Moon, S. Park, T. Chang and C. Chang, *et al.*, *Adv. Funct. Mater.*, 2005, **15**, 77–82.
17 M. Brinkmann and J.-C. Wittmann, *Adv. Mater.*, 2006, **18**, 860–863.

18 S. Joshi, P. Pingel, S. Grigorian, T. Panzner, U. Pietsch, D. Neher, M. Forster and U. Scherf, *Macromolecules*, 2009, **42**, 4651–4660.
19 E. Verploegen, C. E. Miller, K. Schmidt, Z. Bao and M. F. Toney, *Chem. Mater.*, 2012, **24**, 3923–3931.
20 N. Kleinhenz, C. Rosu, S. Chatterjee, M. Chang, K. Nayani, Z. Xue, E. Kim, J. Middlebrooks, P. S. Russo, J. O. Park, M. Srinivasarao and E. Reichmanis, *Chem. Mater.*, 2015, **27**, 2687–2694.
21 N. Kleinhenz, N. Persson, Z. Xue, P. H. Chu, G. Wang, Z. Yuan, M. A. McBride, D. Choi, M. A. Grover and E. Reichmanis, *Chem. Mater.*, 2016, **28**, 3905–3913.
22 D. Choi, S. Jin, Y. Lee, S. H. Kim, D. S. Chung, K. Hong, C. Yang, J. Jung, J. K. Kim, M. Ree and C. E. Park, *ACS Appl. Mater. Interfaces*, 2010, **2**, 48–53.
23 H. Dong, L. Jiang and W. Hu, *Phys. Chem. Chem. Phys.*, 2012, **14**, 14165–14180.
24 L. G. Parratt, *Phys. Rev.*, 1954, **95**, 359–369.
25 M. Tolan, *X-ray Scattering from Soft-Matter Thin Films: Materials Science and Basic Science*, Springer, Berlin, 1998.
26 A. Gibaud and S. Hazra, *Curr. Sci.*, 2000, **78**, 1467–1477.
27 A. Gibaud and G. Vignaud, *X-ray and Neutron Reflectivity: Principles and Applications*, Springer, Berlin, 2009, pp. 85–131.
28 J. K. Bal and S. Hazra, *Phys. Rev. B: Condens. Matter Mater. Phys.*, 2007, **75**, 205411.
29 P. Chatterjee, S. Hazra and H. Amenitsch, *Soft Matter*, 2012, **8**, 2956–2964.
30 I. Roy and S. Hazra, *Soft Matter*, 2015, **11**, 3724–3732.
31 J. K. Bal and S. Hazra, *Phys. Rev. B: Condens. Matter Mater. Phys.*, 2009, **79**, 155412.
32 P. Chatterjee and S. Hazra, *J. Phys. Chem. C*, 2014, **118**, 11350–11356.
33 M. Mukhopadhyay and S. Hazra, *Phys. Chem. Chem. Phys.*, 2018, **20**, 1051–1062.
34 M. Mukhopadhyay and S. Hazra, *Soft Matter*, 2019, **15**, 1869–1878.
35 I. Ahmed, L. Dildar, A. Haque, P. Patra, M. Mukhopadhyay, S. Hazra, M. Kulkarni, S. Thomas, J. R. Plaisier, S. B. Dutta and J. K. Bal, *J. Colloid Interface Sci.*, 2018, **514**, 433–442.
36 S. Mahato, J. Puigdollers, C. Voz, M. Mukhopadhyay, M. Mukherjee and S. Hazra, *Appl. Surf. Sci.*, 2020, **499**, 143967.
37 P.-H. Chu, N. Kleinhenz, N. Persson, M. McBride, J. L. Hernandez, B. Fu, G. Zhang and E. Reichmanis, *Chem. Mater.*, 2016, **28**, 9099–9109.
38 F. C. Spano, *J. Chem. Phys.*, 2005, **122**, 234701.
39 F. C. Spano and C. Silva, *Annu. Rev. Phys. Chem.*, 2014, **65**, 477–500.
40 W. D. Oosterbaan, J.-C. Bolsee, A. Gadisa, V. Vrindts, S. Bertho, J. D'Haen, T. J. Cleij, L. Lutsen, C. R. McNeill, L. Thomsen, J. V. Manca and D. Vanderzande, *Adv. Funct. Mater.*, 2010, **20**, 792–802.
41 J. Y. Na, B. Kang, D. H. Sin, K. Cho and Y. D. Park, *Sci. Rep.*, 2015, **5**, 13288.
42 J. Clark, J.-F. Chang, F. C. Spano, R. H. Friend and C. Silva, *Appl. Phys. Lett.*, 2009, **94**, 163306.
43 S. Tiwari, W. Takashima, S. K. Balasubramanian, S. Miyajima, S. Nagamatsu, S. S. Pandey and R. Prakash, *Jpn. J. Appl. Phys.*, 2014, **53**, 021601.
44 K. Zhao, X. Yu, R. Li, A. Amassian and Y. Han, *J. Mater. Chem. C*, 2015, **3**, 9842–9848.
45 E. S. Manas and F. C. Spano, *J. Chem. Phys.*, 1998, **109**, 8087–8101.
46 J. D. Roehling, I. Arslan and A. J. Moule, *J. Mater. Chem.*, 2012, **22**, 2498–2506.
47 H. Kiessig, *Ann. Phys.*, 1931, **402**, 769–788.
48 I. Roy and S. Hazra, *RSC Adv.*, 2017, **7**, 2563–2572.
49 O. Werzer and R. Resel, *Macromolecules*, 2013, **46**, 3529–3533.
50 N. E. Persson, P.-H. Chu, M. McBride, M. Grover and E. Reichmanis, *Acc. Chem. Res.*, 2017, **50**, 932–942.
51 S. T. Salammal, E. Mikayelyan, S. Grigorian, U. Pietsch, N. Koenen, U. Scherf, N. Kayunkid and M. Brinkmann, *Macromolecules*, 2012, **45**, 5575–5585.
52 M. McBride, G. Bacardi, C. Morales, B. Risteen, D. Keane, E. Reichmanis and M. A. Grover, *ACS Appl. Mater. Interfaces*, 2019, **11**, 37955–37965.